NANO LETTERS

2007
Vol. 7, No. 9
2847−2853

Perylenediimide Nanowires and Their Use in Fabricating Field-Effect Transistors and Complementary Inverters

Alejandro L. Briseno,*,† Stefan C. B. Mannsfeld,‡ Colin Reese,‡ Jessica M. Hancock,† Yujie Xiong,† Samson A. Jenekhe,*,†,§ Zhenan Bao,*,‡ and Younan Xia*,†

Department of Chemistry, University of Washington, Seattle, Washington 98195, Department of Chemical Engineering, Stanford University, Stanford, California 94305, and Department of Chemical Engineering, University of Washington, Seattle, Washington 98195

Received June 22, 2007; Revised Manuscript Received August 2, 2007

ABSTRACT

Perylenetetracarboxyldiimide (PTCDI) nanowires self-assembled from commercially available materials are demonstrated as the n-channel semiconductor in organic field-effect transistors (OFETs) and as a building block in high-performance complementary inverters. Devices based on a network of PTCDI nanowires have electron mobilities and current on/off ratios on the order of 10^{-2} cm^2/Vs and 10^4, respectively. Complementary inverters based on n-channel PTCDI nanowire transistors and p-channel hexathiapentacene (HTP) nanowire OFETs achieved gains as high as 8. These results demonstrate the first example of the use of one-dimensional organic semiconductors in complementary inverters.

One-dimensional (1-D) organic semiconductor nanostructures[1] formed via self-assembly are regarded as a promising class of nanomaterials for use in solution-processable organic field-effect transistors.[2] Although field-effect transistors with excellent performance have been demonstrated by various groups for 1-D nanostructures of p-type organic semiconductors,[3−5] very few examples of OFETs with 1-D n-channel semiconductors have been published, and those reported required high-temperature synthesis.[6] Electron-transporting semiconductors and n-channel OFETs[7] are highly desired, as they will enable the fabrication of complementary inverters, ring oscillators, and shift registers for radio-frequency identification (RFID) tags and complex circuits.[8−11] Among n-type semiconductors, the perylenediimides (PTCDIs) are the most widely studied due to their commercial availability, low cost, chemical stability, and promising electronic and optoelectronic applications.[12] In addition, PTCDIs have a propensity to self-assemble into 1-D nanostructures through $\pi-\pi$ stacking.[1,7a,12,13] Many studies of PTCDI nanowires (NWs) have been reported,[12,13] but we are unaware of any report of their incorporation in OFETs. Here, we report both n-channel OFETs based on PTCDI NWs and complementary inverters achieved by combining them with the p-type hexathiapentacene (HTP)[14] NWs we recently reported.[5] The results of this study show that one can easily fabricate transistors and basic logic elements that exhibit excellent electrical characteristics via solution-processing.

A series of commercially available (from Aldrich) perylenetetracarboxyldiimide (PTCDI−C_n, where $C_n = C_5H_{11}$, C_8H_{17}, $C_{13}H_{27}$) derivatives[7a,15] (Figure 1A) were used for producing NWs via solution-phase self-assembly. The PTCDI−C_n NWs were synthesized by adding methanol to the solutions of PTCDI−C_n in chloroform (∼1.5 mg/mL) to induce the precipitation and self-assembly by $\pi-\pi$ interactions[1,12,13] of PTCDI. Figure 1B shows optical photographs capturing the progression of self-assembly of PTCDI−C_8 NWs. The bottom layer of the vials contains PTCDI dissolved in chloroform and the upper layer contains methanol. An initial swirl of the vial immediately induced the supramolecular self-assembly, and in several minutes, the complete formation of NWs were observed. The synthesis could be performed under similar conditions for all three PTCDI derivatives in bulk quantities (see the last frame in

* Corresponding authors. E-mail: xia@chem.washington.edu (Y.X.); abriseno@u.washington.edu (A.L.B.); jenekhe@u.washington.edu (S.A.J.); zbao@stanford.edu (Z.B.).
† Department of Chemistry, University of Washington.
‡ Department of Chemical Engineering, Stanford University.
§ Department of Chemical Engineering, University of Washington.

10.1021/nl071495u CCC: $37.00
Published on Web 08/16/2007

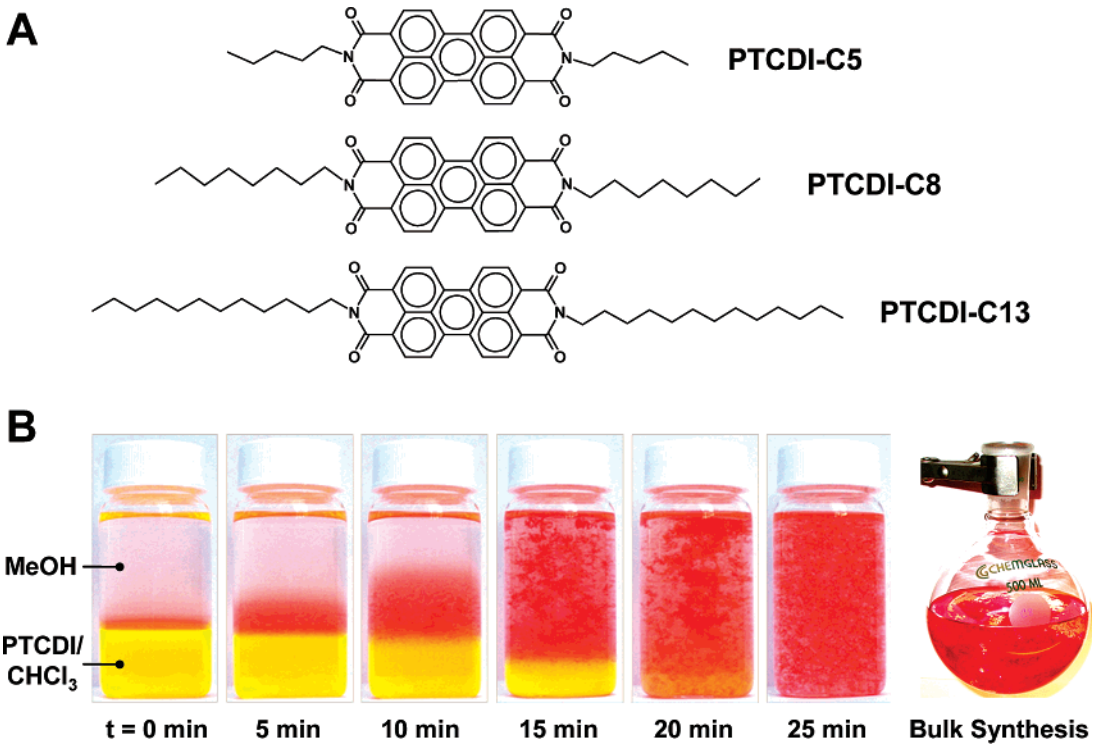

Figure 1. (A) Chemical structures of the three perylenetetracarboxyldiimide (PTCDI) derivatives of varying dialkyl chain lengths synthesized as n-type semiconductor NWs using a solution-phase method. (B) A series of optical photographs detailing the interfacial self-assembly of PTCDI nanostructures. The top layer of the vial is methanol, and bottom layer is PTCDI dissolved in chloroform (~1.5 mg/mL). The last picture frame illustrates a 500 mL flask containing a large quantity of PTCDI−C_8 NWs that were also synthesized in ~25 min.

Figure 1B) in the same time span as for small-scale synthesis. Field-effect transistors and complementary inverters were fabricated by drop-casting the as-prepared NWs in a methanol solution.

We monitored the crystallization of the nanostructures spectroscopically with the same experimental conditions as above and observed interesting absorption spectra (Figure S1, Supporting Information). The absorption spectrum of PTCDI−C_8 in chloroform (t = 0) has a well-resolved vibronic structure with 0−0, 0−1 and 0−2 transitions at 528, 492, and 460 nm, respectively. The normalized absorption spectra taken at different times during the nanowire self-assembly showed shifts in the intensities of the vibronic transitions and the emergence of a new lower energy band centered at 580 nm. The red-shifted new absorption band centered at 580 nm can be assigned to the J-aggregates[16] within the crystalline PTCDI−C_8 NWs.[12] These observations are consistent with previously reported absorption characteristics of similar PTCDI derivatives.[13]

Our attempt to determine the molecular packing and crystallographic orientation[3,4c,5] of PTCDI molecules along individual NWs using transmission electron microscopy (TEM) was unsuccessful due to the significant damage from the electron beam. Although we were still able to acquire faint TEM diffraction spots from single NWs (Figure S3, Supporting Information), the weak signal prevented precise structural analysis and we could only conclude that the NWs are highly crystalline in nature. However, single-crystal X-ray crystallography data were successfully obtained from several millimeter long needles of PTCDI−C_8 that were grown under similar growth conditions as for bulk NWs. The following parameters were determined for the $P\bar{1}$ unit cell containing a single PTCDI−C_8 molecule: a = 4.68 Å, b = 8.50 Å, c = 19.72 Å, α = 85.99°, β = 91.57°, γ = 82.79°. The packing alignment of the PTCDI−C_8 molecule in the unit cell is schematically shown in Figure 2A. The PTCDI−C_8 molecules exhibit slipped $\pi-\pi$ stacking in the [100] direction (a-axis) with the shortest vertical contact between the aromatic planes of neighboring PTCDI−C_8 molecules at 3.24 Å. From the alignment of the single-crystal needle in the diffractometer, it could be inferred that the long needle direction (wire direction) corresponds to the [100] direction. This is in agreement with the Wulff plot of the crystal shape (Figure 2B) that was calculated using the BFDH method.[17] The theoretically predicted PTCDI−C_8 crystal shape is elongated along the [100] direction. Consequently, the overlap of the molecular π orbitals, crucial for the charge transport in organic semiconductor materials, is significant only in the long wire direction. This quasi-one-dimensioanal type of stacking is well-known from other large perylene derivatives[7a,18,19] (including PTCDI−C_5 and PTCDI−C_{13}) and underscores the applicability of PTCDI−C_n NWs for high-performance transistor devices.

Additional characterization of the PTCDI−C_n NWs was carried out using SEM and TEM. Parts A and B of Figure 3 show typical SEM/TEM images of the PTCDI−C_5 NWs. A close examination of the structures reveals a "nanobelt" morphology with an average width of 315 ± 80 nm as determined from the TEM measurements. Parts C and D of Figure 3 also show SEM/TEM images for PTCDI−C_8;

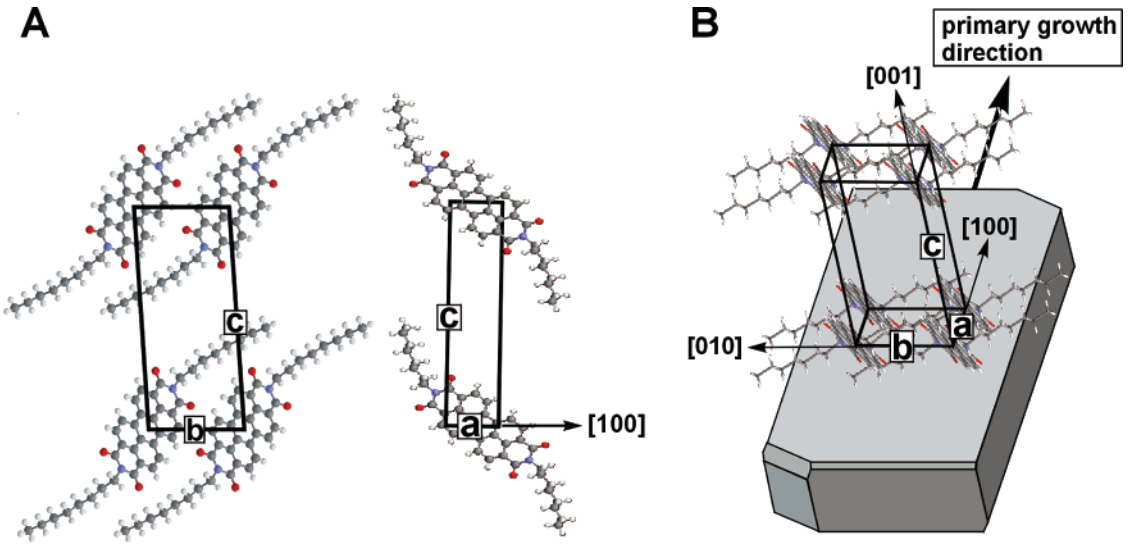

Figure 2. (A) The PTCDI−C_8 unit cell as determined by single-crystal X-ray diffraction for a large crystalline needle. The molecules exhibit slipped $\pi-\pi$ stacking along the [100] direction (see $b-c$ plane), which was experimentally confirmed to correspond to the long axis of the crystalline needle. (B) The theoretically predicted crystal habit (Bravais−Friedel−Donnay−Harker method, BFDH) exhibits an elongation along the [100] direction, which is also in agreement with the observed nanowire growth.

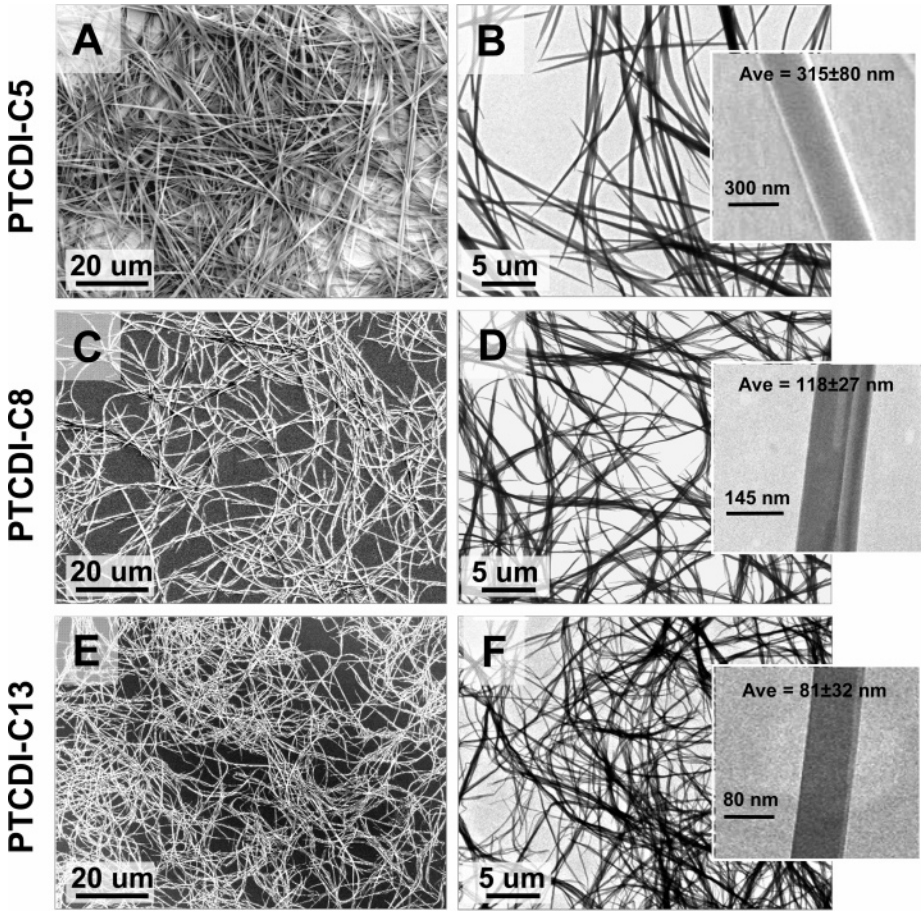

Figure 3. (A,C,E) SEM images and (B,D,F) TEM images of PTCDI NWs. The SEM and TEM images correspond to the respective PTCDI−C_n semiconductor indicated to the left of the frames. The insets show TEM images of representative single nanowires, together with average nanowire widths.

however, the morphology is somewhat different from PTCDI−C_5. PTCDI−C_8 self-assembles into individualized belts with an average width of 118 ± 27 nm and then into bundles. PTCDI−C_{13} also self-assembled into bundles composed of nanobelts but with a narrower width of 81 ± 32 nm (Figures 3E,F). We observed a noticeable difference in the growth trend among the PTCDI−C_n NWs. As the *n*-alkyl chain length increases, the width of the nanowire

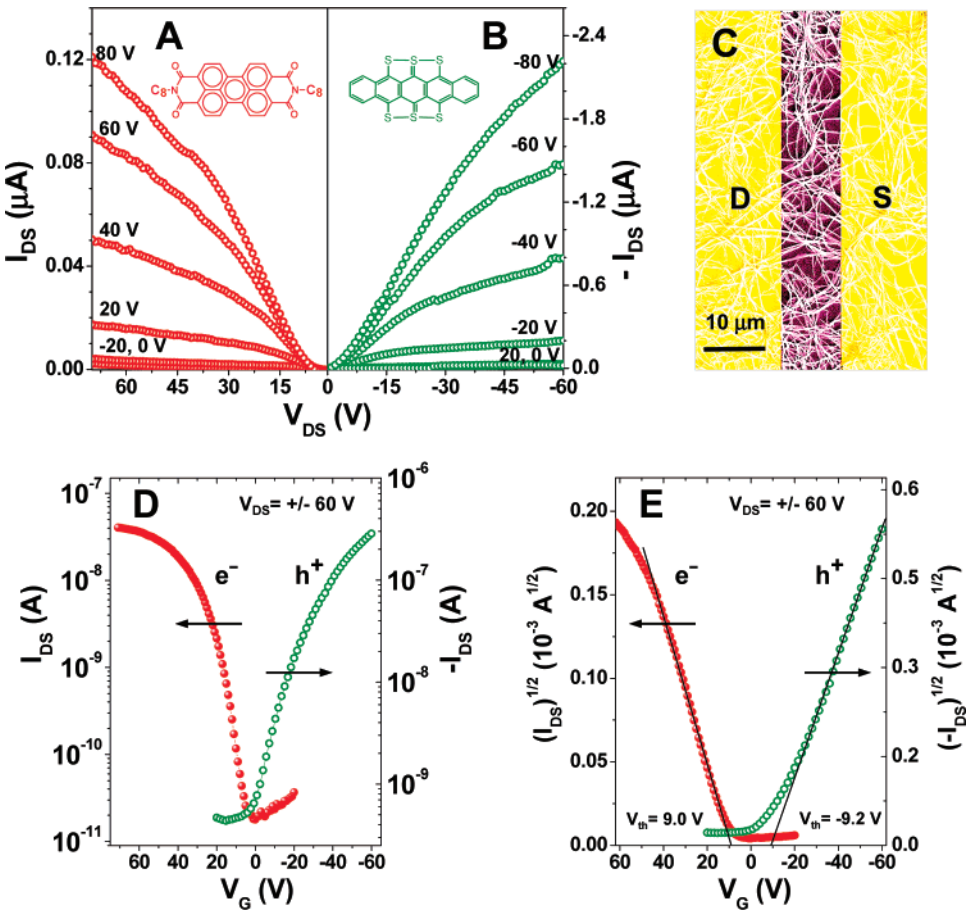

Figure 4. Output characteristics of field-effect transistors fabricated from (A) PTCDI−C_8 and (B) HTP NWs. (C) A colorized SEM image of a network of PTCDI−C_8 NWs drop-cast across the gold electrodes from a methanol suspension. (D) Overlay of transfer characteristics of PTCDI−C_8 and HTP and (E) an overlay of the square root of the drain current with indicated threshold voltages. All measurements on nanowire transistors were made under ambient conditions with a Keithley 4200 SC semiconductor analyzer/probe station.

decreases. A logical explanation is that the longer the *n*-alkyl chain is, the lower solubility it will have as one adds methanol to solutions of PTCDI−C_n in chloroform. Hence, more nucleation sites are formed (more abundant and smaller crystallites) and narrower belts are obtained.

An important goal beyond synthesis of the n-type semiconductor NWs is to fabricate functional arrays of transistors and inverters via solution casting. Therefore, we conducted measurements on n-channel PTCDI−C_n transistors and p-channel hexathiapentacene (HTP) transistors by drop-casting nanowire/methanol solutions onto gold interdigitated electrodes (IDEs) that were fabricated by conventional photolithography. It was imperative to employ IDEs because traditional source−drain electrodes did not generate sufficient output current to record decent data from the PTCDI−C_n nanowire OFETs. IDEs are often utilized when measuring low-mobility materials because the interdigitated source−drain fingers significantly amplify the output current and improve device characteristics[2c,11] without altering the measured mobility of the semiconductor material. The devices were fabricated on highly doped Si substrates as back gates and thermally grown SiO_2 (300 nm) as gate dielectrics with Ti/Au as the bottom-contact source−drain electrodes (*W*/*L* ratios varied but were ∼150 for most devices). All electrical measurements were carried out in ambient air and at room temperature.

Parts A and B of Figure 4 show typical output characteristics of PTCDI−C_8 and HTP nanowire OFETs, respectively. Both devices show significant contact resistance, as evidenced from the nonlinearity of the output curve at low source−drain voltage, and can be attributed to the nonideal semiconductor−metal interface. Figure 4C shows an SEM image of a network of PTCDI−C_8 NWs across two fingers of the IDE with an estimated channel coverage of 50−60%. As shown in the overlay of the transfer characteristics of HTP NWs and PTCDI NWs in Figure 4D, the current on/off ratios were ∼10^3 for the p-channel and n-channel OFETs. Figure 4E shows the square root of the saturated drain current versus the gate voltage for the HTP nanowire and PTCDI nanowire OFETs. The relatively small threshold voltage for both devices results in a significantly narrow gate voltage difference between the two threshold voltages, enabling good characteristics for the complementary inverter devices. The similar OFET threshold voltages suggest HTP and PTCDI are good candidates for the design of complementary devices. From the saturation-regime transfer plots, we estimate[20] electron mobilities of $6.9 \pm 2.7 \times 10^{-5}$, $7.2 \pm 7.0 \times 10^{-3}$, and $6.7 \pm 3.0 \times 10^{-3}$ cm^2/Vs for PTCDI−C_5, −C_8, and

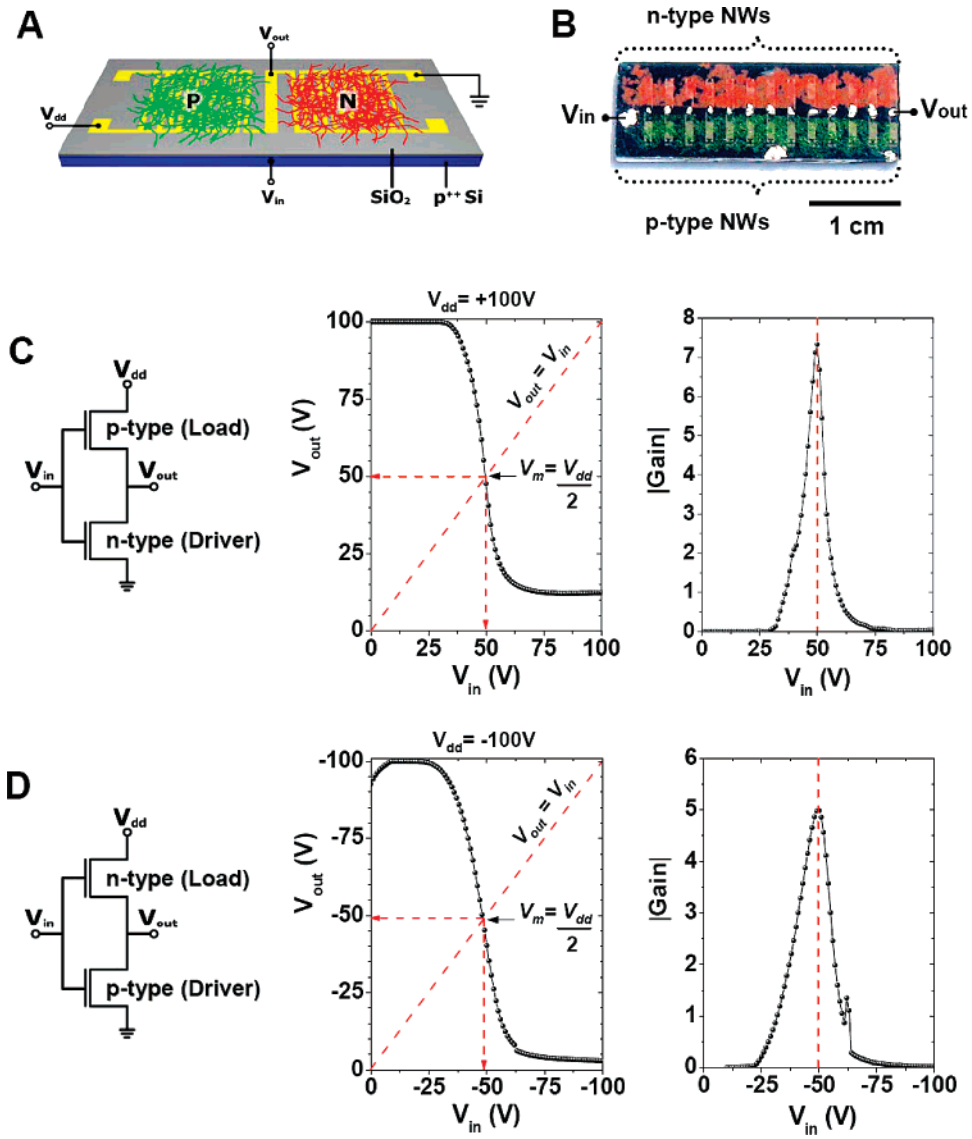

Figure 5. (A) Schematic of an inverter with p- and n-type nanowire networks covering interdigitated source−drain electrodes, and (B) a photograph of a substrate containing 13 discrete inverters. Nanowires were drop-cast onto individual transistor devices from a methanol/nanowire solution. (C) Static inverter transfer characteristics with the p-channel OFET as the load and the n-channel OFET as the driver, with the configuration reversed in (D). The frames to the right show the corresponding voltage gain in the transition region where the gate threshold voltage is located. These results correspond to one of our best performing inverters.

$-C_{13}$, respectively. The highest mobility measured was 0.027 cm^2/Vs for PTCDI$-C_8$ (Table S5, Supporting Information). Mobility values for HTP OFETs are on the order of 10^{-2} to 10^{-3} cm^2/Vs.[5] We were unable to measure any functional devices from solution-cast thin-film transistors of the PTCDI$-C_5$, $-C_8$, $-C_{13}$ derivatives in ambient air. Remarkably, the n-type nanowire devices were all measured in air and remained functional for several days with performance declining thereafter (with the exception of PTCDI$-C_5$, which remained functional for only several hours). The devices can easily be regenerated by heating to 130 °C for 15 min in a vacuum oven. Previous PTCDI$-C_n$ thin-film transistors from similar materials were reportedly measured either under vacuum or an inert atmosphere and ceased to operate when measured in air.[7a,10a,15] This suggests that moisture trapping at the nanowire/dielectric interface may be the primary reason for the degradation of the device performance. Although our nanowire TFTs were not measured in vacuum or inert atmospheres, we expect electron mobilities to be significantly larger under these conditions. As a final note, it is not a surprise to see that the electron mobility increases as the alkyl chain length increases. This trend in performance is consistent with literature values for TFTs fabricated from the same materials where PTCDI$-C_5$ < PTCDI$-C_8$ ≤ PTCDI$-C_{13}$. For instance, the electron mobilities in literature for PTCDI$-C_5$, $-C_8$, and $-C_{13}$ thin-film transistors are on the order of 0.1 cm^2/Vs,[7a] 0.6−1.7 cm^2/Vs,[7a,15c] and 2.1 cm^2/Vs,[15a] respectively. Although the electron mobilities of these materials are much larger than our nanowire TFTs (due to highly optimized conditions), the general trend in performance remains consistent. While there is no obvious difference in the molecular packing among the three PTCDI molecules,[7a] one can speculate that the longer alkyl-chain-containing PTCDI molecules interdigitate more efficiently

in the solid-state and reduce the penetration of environmental contaminants such as water or molecular oxygen. This solid-state packing effect has been previously suggested in explaining the behavior in air stability for highly crystalline n-channel organic TFTs.[21] Therefore, based on this premise, there are likely to be fewer traps and/or defects in the crystals from the materials with longer alkyl chains, thus higher performance is expected. The inherently lower mobility of PTCDI−C_5 TFTs (both in thin-film form and in nanowire form) may also be attributed to the intrinsic transport properties of this material.

We fabricated arrays of inverters from the n-channel and p-channel nanowire transistors. Figure 5A shows a schematic of the inverter, with n- and p-type nanowire networks covering interdigitated source−drain gold electrodes. Figure 5B shows a photograph of one of the actual devices used in the measurements; this particular device contains an array of 13 discrete inverters with the same device configuration shown in Figure 5A. The metallic spots along the device array in Figure 5B are indium slugs placed directly onto the two drain electrodes (V_{out}) for probing purposes. A common gate (highly doped Si) functions as the input node (V_{in}) while the source of the driver is grounded and the source of the load transistor is providing the supply voltage (V_{dd}). Figure 5C shows the static voltage-transfer characteristics, i.e., dc transfer characteristics, which plots the output voltage as a function of input voltage, $V_{out} = f(V_{in})$. An important characteristic to consider is the gate or switching threshold voltage (V_m), which should not be confused with the threshold voltage (V_{th}) of a transistor.[20] The gate switching threshold, V_m, is the midpoint of the switching characteristics where both devices are "on" momentarily. This attribute of complementary inverters greatly reduces power consumption (i.e., low static power dissipation) as compared to other electronic devices[8] and has enabled them as the most widely used circuits in modern microelectronics technology. This value can be graphically determined at the intersection of the transfer curve (Figure 5C,D) and the line given by $V_{out} = V_{in}$. Figure 5C demonstrates adequate voltage gains, as obtained from the derivative of the voltage-transfer characteristic in the switching threshold region. The gain is further defined as the maximum small-gain amplification.[8] Several of our inverters exhibit nearly symmetrical voltage-transfer curves and gate switching (e.g., $V_m = V_{dd}/2 = \sim 50$ V), and the results were similar when the configuration was reversed. For example, it is possible to exchange the load (p-type) and driver (n-type) polarity by electrically connecting the supply voltage to the n-channel transistor (now the load) and grounding the p-channel OFET (now the driver), as shown in the circuit configurations accompanying Figure 5C,D. The voltage-controlled devices demonstrate switching from high to low states, the basic logic bit consisting of "1" and "0". Remarkably, our inverters still demonstrate good threshold switching voltages upon exchanging the two transistors, which can be attributed to the equal current-driving strengths in both directions. Matching of device performance (i.e., mobilities) and similar (but opposite in voltage polarity) threshold voltages also contributes to well-resolved characteristics.[8,9] Channel dimensions and geometries offer additional flexibility in improving the inverter transfer characteristics.[8b] For instance, if one of the two transistors has different mobilities or low output currents, the device geometry may be adjusted to obtain comparable drive currents for both transistors. IDEs, for which overall W/L is adjustable, are therefore critical for generating well-resolved transfer characteristics (Figure 5C,D) and relatively large voltage gains for materials of varying performance. We note that standard source−drain electrodes with the n-type PTCDI nanowire networks did not generate well-resolved electrical characteristics or useful data.

In conclusion, by combining n-channel (PTCDI) and p-channel (HTP) nanowire transistors, we have demonstrated logic functionality in the form of a basic complementary inverter. We were able to accomplish this by synthesizing large quantities of crystalline NWs from a variety of low-cost, commercially available, n-type PTCDI−C_n semiconductors via a solution-phase process. Because this is one of the first examples of the utilization of 1-D organic nanostructures in complementary logic circuits, we believe these findings will contribute to the development of organic electronics.

Acknowledgment. A.L.B. thanks the Bell Labs for a Graduate Research Fellowship. S.C.B.M. acknowledges a postdoctoral fellowship from the Deutsche Forschungsgemeinschaft (DFG, grant MA 3342/1-1). Y.X. acknowledges partial support from GEMSEC, an NSF-supported MRSEC program at the UW. S.A.J. acknowledges support from the NSF (CTS-0437912), the NSF STC-CMDITR (DMR-0120967), and the Air Force Office of Scientific Research (AFOSR) (grant F49620-03-1-0162). Z.B. acknowledges partial support from the Stanford NSF-MRSEC Center for Polymeric Interfaces and Macromolecular Assemblies (DMR-0213618) and the AFOSR grant FA9550-06-1-0126. We acknowledge Shuhong Liu, Harvey Ho, Prof. Babak Parviz, and F. Sunjoo Kim for their assistance with device fabrication, and we thank Dr. Werner Kaminsky for determining the X-ray crystal structure of PTCDI−C_8. We also acknowledge the Nanotech User Facility (NTUF), a member of the National Nanotechnology Infrastructure Network (NNIN) funded by the NSF.

Supporting Information Available: Additional results and X-ray crystallographic data (CIF). This material is available free of charge via the Internet at http://pubs.acs.org.

Note Added after ASAP Publication. The unit of measure for electron mobility appeared with the number for the on/off ratio in the abstract of the version published ASAP August 16, 2007; the corrected version was published ASAP August 24, 2007.

References

(1) (a) Meijer, E. W.; Schenning, A. P. H. J. *Nature* **2002**, *419*, 353. (b) Hoeben, F. J. M.; Jonkheijm, P.; Meijer, E. W.; Schenning, A. P. H. J. *Chem. Rev.* **2005**, *105*, 1491.

(2) (a) Chabinyc, M. L.; Salleo, A. *Chem. Mater*. **2004**, *16*, 4509−4521. (b) Forrest, S. *Nature* **2004**, *428*, 911−918. (c) Stingelin-Stutzmann, N.; Smits, E.; Wondergem, H.; Tanase, C.; Blom, P.; Smith, P.; de Leeuw, D. *Nat. Mater*. **2005**, *4*, 601−606. (d) Katz, H. E.; Bao, Z.; Gilat, S. L. *Acc. Chem. Res*. **2001**, *34*, 359−369. (e) Anthony, J. E. *Chem. Rev*. **2006**, *106*, 5028−5048. (f) Ong, B. S.; Wu, Y.; Liu, P.; Gardner, S. *J. Am. Chem. Soc.* **2004**, *126*, 3378−3379.

(3) (a) Xiao, S.; Tang, J.; Beetz, T.; Guo, X.; Tremblay, N.; Siegrist, T.; Zhu, Y.; Steigerwald, M.; Nuckolls, C. *J. Am. Chem. Soc*. **2006**, *128*, 10700−10701. (b) Tang, Q.; Li, H.; He, M.; Hu, W.; Liu, C.; Chen, K.; Wang, C.; Liu, Y.; Zhu, D. *Adv. Mater.* **2006**, *18*, 65−68. (c) Tang, Q.; Li, H.; Song, Y.; Xu, W.; Hu, W.; Jiang, L.; Liu, Y.; Wang, X.; Zhu, D. *Adv. Mater*. **2006**, *18*, 3010−3014.

(4) (a) Briseno, A. L.; Roberts, M.; Ling, M.-M.; Moon, H.; Nemanick, E. J.; Bao, Z. *J. Am. Chem. Soc*. **2006**, *128*, 3880−3881. (b) Lee, W. H.; Kim, D. H.; Jang, Y.; Cho, J. H.; Hwang, M.; Park, Y. D.; Kim, Y. H.; Han, J. I.; Cho, K. *Appl. Phys. Lett*. **2007**, *90*, 132106. (c) Kim, D. H.; Lee, D. Y.; Lee, H. S.; Lee, W. H.; Kim, Y. H.; Han, J. I.; Cho, K. *Adv. Mater.* **2007**, *19*, 678−682.

(5) Briseno, A. L.; Mannsfeld, S. C. B.; Liu, X.; Xiong, Y.; Jenekhe, S. A.; Bao, Z.; Xia, Y. *Nano Lett.* **2007**, *7*, 668−675.

(6) Tang, Q.; Li, H.; Liu, Y.; Hu, W. *J. Am. Chem. Soc.* **2006**, *128*, 14634−14639.

(7) (a) Chesterfield, R. J.; McKeen, J. C.; Newman, C. R.; Ewbank, P. C.; da Silva Filho, D. A.; Bredas, J.-L.; Miller, L. L.; Mann, K. R.; Frisbie, C. D. *J. Phys. Chem. B* **2004**, *108*, 19281−19292. (b) Newman, C. R.; Frisbie, C. D.; da Silva Filho, D. A.; Bredas, J.-L.; Ewbank, P. C.; Mann, K. R. *Chem. Mater*. **2004**, *16*, 4436−4451. (c) Babel, A.; Jenekhe, S. A. *J. Am. Chem. Soc.* **2003**, *125*, 13656−13657.

(8) (a) Klauk, H.; Zschieschang, U.; Pflaum, J.; Halik, M. *Nature* **2007**, 445, 745−748 and references therein. (b) Crone, B.; Dodabalapur, A. In *Printed Organic and Molecular Electronics*; Gamota, D. R., Brazis, P., Kalyanasundaram, K., Zhang, J., Eds.; Kluwer Academic: Boston, 2003; Chapter 4.3, p 493. (c) Meijer, E. J.; De Leeuw, D. M.; Setayesh, S.; Van Veenendaal, E.; Huisman, B.-H.; Blom, P. W. M.; Hummelen, J. C.; Scherf, U.; Klapwijk, T. M. *Nat. Mater*. **2003**, *2*, 678.

(9) (a) Clemens, W.; Fix, W. W.; Ficker, J.; Knobloch, A.; Ullmann, A. *J. Mater. Res.* **2004**, *19*, 1963−1973. (b) Baude, P. F.; Ender, D. A. D. A.; Haase, M. A.; Kelley, T. W.; Muyres, D. V.; Theiss, S. D. *Appl. Phys. Lett*. **2003**, *82*, 3964. (c) Crone, B. K.; Dodabalapur, A.; Sarpeshkar, R.; Filas, R. W.; Lin, Y.-Y.; Bao, Z.; O'Neill, J. H.; Li, W.; Katz, H. E. *J. Appl. Phys.* **2001**, *89*, 5125. (d) Crone, B.; Dodabalapur, A.; Lin, Y. Y.; Filas, R. W.; Bao, Z.; Sarpeshkar, R.; Katz, H. E.; Li, W. *Nature* **2000**, *403*, 521. (e) Singh, Th. B.; Senkarabacak, P.; Sariciftci, N. S.; Tanda, A.; Lackner, C.; Hagelauer, R.; Horowitz, G. *Appl. Phys. Lett*. **2006**, *89*, 033512.

(10) (a) Gundlach, D. J.; Pernstich, K. P.; Wilckens, G.; Gruter, M.; Haas, S.; Batlogg, B. *J. Appl. Phys.* **2005**, *98*, 064502/1−064502/8. (b) Ling, M.-M.; Bao, Z.; Erk, P.; Koenemann, M. *Appl. Phys. Lett*. **2007**, *90*, 093508.

(11) Briseno, A. L.; Tseng, R. J.; Li, S.-H.; Chu, C.-W.; Yang, Y.; Falcao, E. H. L.; Wudl, F.; Ling, M.-M.; Chen, H. Z.; Bao, Z.; Meng, H.; Kloc, Ch. *Appl. Phys. Lett*. **2006**, *89*, 222111.

(12) Würthner, F. *Chem. Commun.* **2004**, *14*, 1564.

(13) (a) Balakrishnan, K.; Datar, A.; Oitker, R.; Chen, H.; Zuo, J.; Zang, L. *J. Am. Chem. Soc*. **2005**, *127*, 10496. (b) Datar, A.; Balakrishnan, K.; Yang, X.; Zuo, X.; Huang, J.; Oitker, R.; Yen, M.; Zhao, J.; Tiede, D. M.; Zang, L. *J. Phys. Chem. B* **2006**, *110*, 12327−12332. (c) Che, Y.; Datar, A.; Balakrishnan, K.; Zang, L. *J. Am. Chem. Soc.* **2007**, *129*, 7234−7235.

(14) Briseno, A. L.; Miao, Q.; Ling, M.-M.; Reese, C.; Meng, H.; Bao, Z.; Wudl, F. *J. Am. Chem. Soc*. **2006**, *128*, 15576−15577.

(15) (a) Tatemichi, S.; Ichikawa, M.; Koyama, T.; Taniguchi, Y. *Appl. Phys. Lett*. **2006**, *89*, 112108. (b) Rost, C.; Gundlach, D. J.; Karg, S.; Riess, W. *J. Appl. Phys.* **2004**, *95*, 5782. (c) Malenfant, P. R. L.; Dimitrakopoulos, C. D.; Gelorme, J. D.; Kosbar, L. L.; Graham, T. O.; Curioni, A.; Andreoni, W. *Appl. Phys. Lett.* **2002**, *80*, 2517−2519. (d) Chesterfield, R. J.; Mckeen, J. C.; Newman, C. R.; Frisbie, C. D.; Ewbank, P. C.; Mann, K. R.; Miller, L. L. *J. Appl. Phys.* **2004**, *95*, 6396.

(16) Pope, M.; Swenberg, C. E. *Electronic Processes in Organic Crystals and Polymers*, 2nd ed.; Oxford University Press: New York, 1999; pp 39−48.

(17) Donnay, J. D. H.; Harker, D. *Am. Mineral.* **1937**, *22*, 463.

(18) Engel, E.; Koschorreck, M.; Leo, K.; Hoffmann, M. *Phys. Rev. Lett.* **2005**, *95*, 157403.

(19) Hoffmann, M.; Schmidt, K.; Fritz, T.; Hasche, Agranovich, T. V. M.; Leo, K. *Chem. Phys.* **2000**, *258*, 73.

(20) The field-effect mobility was calculated in the saturation region from the equation, $I_{DS} = (W \cdot C \cdot \mu/2 \cdot L)(V_G - V_{th})^2$, where the capacitance, $C = 10$ nF/cm^2 for 300 nm thick SiO_2 gate dielectric and V_{th} is the threshold voltage.

(21) (a) Katz, H. E.; Johnson, J.; Lovinger, A. J.; Li, W. J. *J. Am. Chem. Soc.* **2000**, *122*, 7787. (b) Ling, M.-M.; Erk, P.; Gomez, M.; Koenemann, M.; Locklin, J.; Bao, Z. *Adv. Mater*. **2007**, *19*, 1123−1127.

NL071495U